Surface barrier in Hg-based polycrystalline superconductors

Yang Ren Sun
National High Magnetic Field Laboratory, Florida State University, Tallahassee, Florida 32306-4005

J. R. Thompson
Solid State Division, Oak Ridge National Laboratory, P.O. Box 2008, Oak Ridge, Tennessee 37831-6061
and Department of Physics, The University of Tennessee, Knoxville, Tennessee 37996-1200

J. Schwartz
National High Magnetic Field Laboratory and College of Engineering, Florida State University, Tallahassee, Florida 32306-4005
and Department of Mechanical Engineering, Florida A&M University, Tallahassee, Florida 32308

D. K. Christen
Solid State Division, Oak Ridge National Laboratory, P.O. Box 2008, Oak Ridge, Tennessee 37831-6061

Y. C. Kim
Department of Physics, The University of Tennessee, Knoxville, Tennessee 37996-1200

M. Paranthaman
Chemical and Analytical Sciences Division, Oak Ridge National Laboratory, P.O. Box 2008, Oak Ridge, Tennessee 37831-6100
(Received 14 July 1994)

Pronounced effects of a surface barrier are frequently observed on polycrystalline superconductors of $HgBa_2Ca_{n-1}Cu_nO_{2n+2+\Delta}$ [Hg-12$(n-1)n$] with $n=1$, 2, and 3. Compared with other known high-temperature superconductors, the effects at low temperatures are much stronger and persist over a wide range of magnetic fields. The present analysis shows that the enhancement of the irreversible magnetization of grains by the surface barrier is comparable to that by neutron irradiations. The magnitude of the surface supercurrent density is $>4\times10^7$ A/cm^2 at $T=40$ K and $H=45$ kG, for Hg-1223. The upper and lower boundaries of the thickness of the vortex-free region and the surface-current density are analyzed as functions of temperature and field.

INTRODUCTION

The recent discovery[1] of mercury-based copper oxide high-temperature superconductors (HTSC) has generated considerable excitement in the superconductivity community. Intensive studies have revealed many properties of the novel materials. These include: identification of the crystal structures that provided an important parameter, the interlayer distance between CuO(1) layers,[2] the penetration depth and coherence length of Hg-1201 in the *a-b* plane;[3] and the magnetic irreversibility line of polycrystalline Hg-1201 (Ref. 4) and Hg-1212.[5] Furthermore, the great enhancement of critical current densities in Hg-1201 by neutron irradiation[6] and the elevation of the transition temperatures T_c under quasihydrostatic pressures for all Hg-12$(n-1)n$ superconductors[7] have attracted special attention. In a recent study,[8] we reported the observation of strong pinning effects by a surface barrier in polycrystalline Hg-1201. Here we present a further study on polycrystalline samples of Hg-1212 and Hg-1223. We found that strong surface pinning is a common feature for all Hg-based polycrystalline superconductors.

The nature of the surface barrier was discussed by Bean and Livingston[9] and de Gennes.[10] It was further developed by Clem,[11] Ternovskii, and Shekhata[12] and Burlachkov.[13] The effect is due in part to an attractive interaction between a nucleated vortex line near the sample surface and the material boundary, which is equivalent to a mirror image of the entering vortex line. For an ideal surface, the interaction resists the entry of vortices until the applied magnetic field reaches the value of $H_p=\Phi_0/4\pi\lambda\xi\approx H_c\gg H_{c1}$; here Φ_0 is the flux quantum, λ is the penetration depth, ξ is the coherence length, H_c is the thermodynamical critical field, and H_{c1} is the lower critical field. In most cases, the attraction by the vortex-image is diminished by surface roughness, which leads to the condition $H_{c1}<H_p<H_c$. For $H>H_p$, in which case one has the internal flux density $B>0$, the surface barrier still impedes the entry and exit of vortices, resulting in a magnetization that decays slowly toward its equilibrium value.

The paper is organized as follows. First, evidence of the surface barrier in Hg-1223 and Hg-1212 polycrystalline samples is presented. Next, the results are compared to other high-temperature superconductors, especially $YBa_2Cu_3O_7$, to show the surface barrier in Hg-based superconductors is distinctive. Finally we analyze the temperature and field dependence of both the thickness of the vortex-free region and the density of the supercurrent

flowing in the region. The analysis shows that up to $T=40$ K and $H=45$ kG, a thin surface sheath with thickness less than 25 nm carries a surface current with density larger than 4×10^7 A/cm^2.

EXPERIMENTAL ASPECT

Six randomly oriented polycrystalline samples of Hg-1212 and Hg-1223, three of each sort, were used in the study. Two of each type were synthesized by Wagner and Hinks at Argonne National Laboratory.[2] Among them, one Hg-1212 and one Hg-1223 sample were irradiated with neutrons having $E>0.1$ MeV to a fluence of 2×10^{17} neutrons/cm^2 at the University of Illinois Advanced TRIGA reactor facility.[14] Details on the effects of neutron irradiation will be reported elsewhere. Since the irradiated and the nonirradiated samples were made in the same batch and their preirradiation characteristics were identical, we treat them as one sample and denote the results as the data for the nonirradiated and the irradiated samples. The samples are labeled as $A2$ and $A3$ for Hg-1212 and Hg-1223, respectively. Another two samples, labeled as $O2$ (Hg-1212) and $O3$ (Hg-1223), were prepared at the Chemistry Division, Oak Ridge National Laboratory. The materials were synthesized using the solid-state reaction methods in a single reaction step between previously prepared precursor materials. Details of the sample preparation have been reported elsewhere.[2,15] Characterizations of the mass, grain size, phase purity, and transition temperature of each sample are listed in Table I. The mass volumes, i.e., mass/theoretical density, were used in the calculations to obtain the values of magnetization. Sample $A2$ and $A3$ are irregular shaped, with approximately the same size for length, width and thickness. Sample $O2$ and $O3$ are cylinders of ~2 mm diameter and ~3 mm length. The dc magnetic measurements were conducted using commercial superconducting quantum interference device (SQUID) magnetometers (Quantum Design MPMS-7 and MPMS-5). For measurements of hysteresis loops $M(H)$, the sample was first cooled from above T_c at zero field (ZFC) to the desired temperature and then the field was applied. Flux-creep studies $M(t)$ established the decay with time of induced supercurrents at fixed temperatures and magnetic fields. Each creep measurement lasted about 3 h. For flux entry into the sample, the field was swept directly from zero to the target value, after which the flux creep was measured. For flux exit, H was swept first to some considerably higher field and then decreased to the target value, always ensuring that the flux front penetrated the material fully.

TABLE I. Summary of physical data for Hg-based high-temperature superconducting samples, including average grain size $\langle d_g \rangle$.

Sample	Composition	Phase purity	Mass (mg)	$\langle d_g \rangle$ (μm)	T_c (K)
$A2$ not irradiated	$HgBa_2Ca_1Cu_2O_{6+\Delta}$		129	8	127
$A2$ n irradiated	$HgBa_2Ca_1Cu_2O_{6+\Delta}$		13	8	127
$A3$ not irradiated	$HgBa_2Ca_2Cu_3O_{8+\Delta}$		50	10	135
$A3$ n irradiated	$HgBa_2Ca_2Cu_3O_{8+\Delta}$		16	10	135
$O2$	$HgBa_2Ca_1Cu_2O_{6+\Delta}$	95%	36	6	123
$O3$	$HgBa_2Ca_2Cu_3O_{8+\Delta}$	90%	28	6	134

EXPERIMENTAL RESULTS AND DISCUSSION

The magnetic hysteresis loops $M(H)$ for sample $A3$ before the irradiation at $T=30$, 35, and 40 K are plotted in Fig. 1. Similar data at $T=15$, 20, and 30 K from sample $O2$ are presented in the inset. The most pronounced feature in both plots is the very symmetric curves in the "field-increasing" branch versus the "field-decreasing" branch. In the field-increasing branch of both samples, M develops linearly with increasing field until it reaches a peak value near $H\approx1500$ G, after which M drops quickly. In the field-decreasing branch, the curves of $M(H)$ are very flat and horizontal with values close to zero until H decrease to ~800 G. This asymmetric shape completely conflicts with the Bean model,[16] which predicts a magnetic hysteresis loop that is symmetric about the $M=0$ axis. The small magnetization in the field-decreasing branch is a "fingerprint"[11,13] indicating that surface pinning, rather than bulk pinning, dominates the magnetic behavior. Similar features were found in sample $O2$ and $O3$. Among these samples, $A2$ before the irradiation had the least asymmetric hysteresis loops, but largest width ΔM (the corresponding magnetic J_c was 9×10^6 A/cm^2 at $T=5$ K and zero field). This signifies a relatively lower ratio of surface pinning versus bulk pinning. As we illustrate later, this is due to higher bulk pinning rather than weaker surface pinning.

Flux-creep measurements were conducted on the samples to check the differences of the magnetic relaxation rate $R=dM/d\ln t$ for flux during entry and exit. For a bulk-pinning-dominated system, the theory predicts[17]

$$R=\pm R_0(1\pm\delta)\ , \tag{1}$$

where $\pm$ signs refer to positive or negative ∇B, corresponding to the flux entry or exit in the field-increasing and decreased branches, respectively. According to the theory, $\delta\ll1$. On the other hand, for a surface-pinning-controlled system, the ratio of R_+/R_- depends on the stage of the relaxation.[13] Theoretically, the ratio tends to unity as time t goes to infinity. However, for a time window of practical scale, R_+ is always larger than R_-. A nonlogarithmic decay was found in these samples. Especially at higher fields, the curves of M versus $\ln(t)$ are significantly "bent" in the early stage of relaxation. There is a crossover at $t\sim200$ sec, depending on the field and temperature, after which the curve becomes much more linear. The interpretation of this nonlogarithmic decay is not clear at this moment; it may be due to some similar reasons in bulk-pinning-controlled HTSC (Refs. 18–20) or to the contribution from surface pinning,[13] or

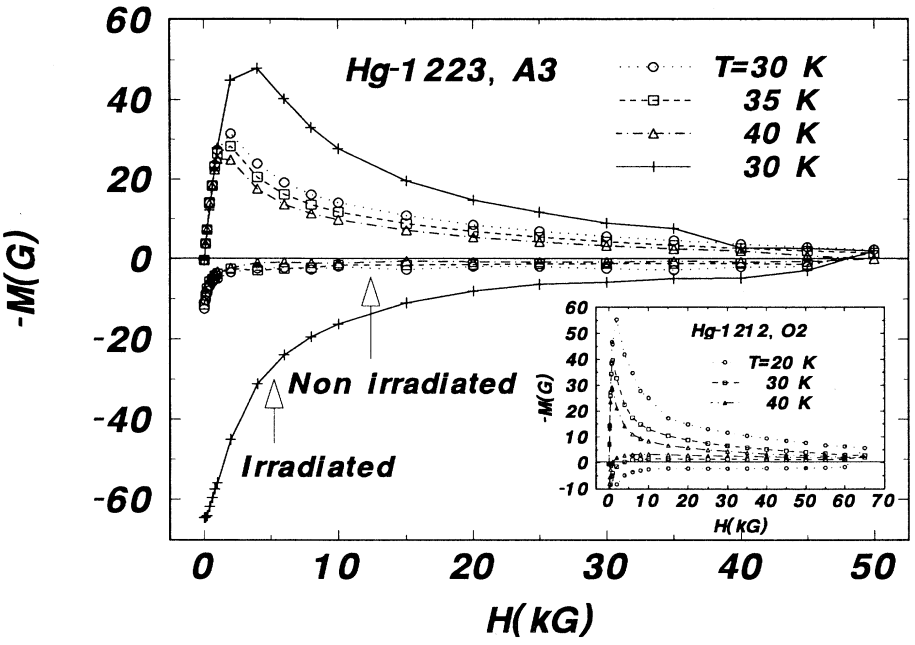

FIG. 1. Magnetization M versus field H for sample $A3$ at $T=30$, 35, and 40 K before neutron irradiation and at $T=30$ K after the irradiation; inset: M versus H at $T=20$, 30, and 40 K for sample $O2$. Lines are guides to the eye.

conceivably some instrumental transient. In addition, it is generally difficult to determine the precise time origin (defined as the time at which the applied field reached the target value) for each relaxation measurement in SQUID magnetometers. To define R clearly and avoid these complications, the values of R_+ and R_- were obtained in the time window of $t > 800$ s where the influence from the inaccuracy of the time origin should be much reduced. In Fig. 2, the ratios of R_+/R_- of sample $A3$ are plotted as a function of field at $T=30$ K. Before the irradiation, R_+ is about 2 or 3 times larger than R_-, which is much greater than what is expected for a bulk-pinning-controlled system. Similar features are seen for measurements taken at other temperatures and for other samples, showing that surface-barrier effects are pronounced and pervasive in these materials.

Another demonstration of the relative importance of the strong surface barrier is that the features mentioned above are greatly reduced or disappeared after increasing the bulk pinning by irradiating with neutrons. To show this point, Fig. 1 includes, for comparison, the magnetization $M(H)$ at $T=30$ K after irradiation. Irradiation significantly reduced the asymmetry of the hysteresis loop so that the magnetization curve in the field-decreasing branch is no longer horizontal nor zero. In addition, the ratios R_+/R_- from relaxation measurements declined markedly (Fig. 2). The coincidence of these changes upon neutron irradiation is a further confirmation that they are correlated events and were associated with an increase of surface roughness and bulk pinning, both due to the irradiation. The effects of irradiation are quite peculiar for sample $A2$. In Fig. 3, hysteresis loops $M(H)$ at $T=20$ K before and after the irradiation are plotted. While irradiation enhanced the magnetization M in the field-decreasing branch over almost the entire region, *M diminished* over a wide region for the other branch. Generally, the enlargement of magnetization is symmetric; irradiation does not degrade the

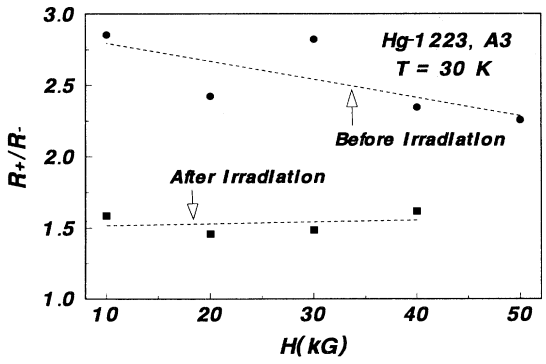

FIG. 2. Ratio of magnetization decay rates R_+/R_- versus magnetic field H at $T=30$ K for sample $A3$, where R_+ represents $dM/d\ln(t)$ in the field increasing branch and R_- in the field decreasing branch.

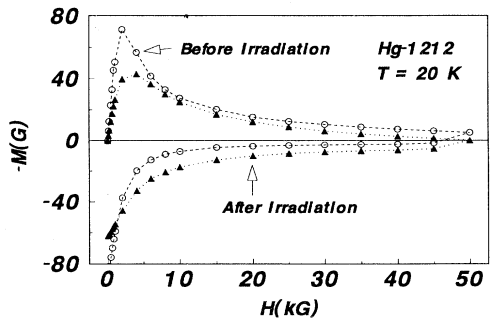

FIG. 3. M versus H for sample at $T=20$ K before and after neutron irradiation with 2×10^{17} n/cm^2.

mixed-state irreversible magnetization unless the dosage is so high that the overall superconductivity of the sample is significantly destroyed. Here we can rule out this possibility, as the T_c of the sample was not affected by the irridation and the magnetization in the field-decreasing branch is enlarged. Our explanation is the following. The hysteresis loop becoming much more symmetric indicates that the surface barrier becomes negligible after the irradiation. Strengthening of the bulk pinning by the irradiation is clearly marked by the enlargement of the magnetization in the field-decreasing branch. In the field-increasing branch, however, destruction of the surface magnetization mainly canceled out the increase in bulk magnetization. Since the surface-barrier-dominated magnetization in the field-decreasing branch was rather small ($M \sim 0$) before irradiation, the net increment in this magnetization becomes prominent. The experiment showed that the effects of the surface barrier before irradiation are comparable with bulk pinning generated by neutron irradiation. Noting that the hysteresis loops of sample $A2$ were the least asymmetric among four unirradiated samples, the above discussion clearly indicates that a stronger bulk pinning but not a weaker surface barrier diminished the apparent effects of surface pinning.

Further evidence for a surface barrier can be obtained via ac response measurements,[8] where the ac magnetic moment is recorded as a function of the magnitude of a small ac field that is coaxially superimposed on a dc field. For a polycrystalline sample of Hg-1201, our previous study has shown excellent agreement between the experimental results and theoretical calculations based upon surface pinning. Since the overall features of dc magnetic measurements for Hg-1223 and Hg-1212 samples are identical to the Hg-1201 sample, it is entirely reasonable to think that the observed phenomena in all three samples (i.e., Hg-1201, Hg-1223, and Hg-1212) stem from the same origin.

A number of questions arise: Why do the Hg-based HTSC materials exhibit such pronounced surface-barrier effects? Are similar features common in other HTSC's? In the following, we contrast the present results with studies performed on a specially chosen polycrystalline sample of $YBa_2Cu_3O_{7-\delta}$ (YBCO).

Observations of surface barriers in $YBa_2Cu_3O_{7-\delta}$ (Refs. 21 and 22) and $Bi_2Sr_2CaCu_2O_8$ (Ref. 23) (BSCCO) single crystals have been reported. However, most experiments were conducted in small fields (~ 100 G) and at temperatures either near to T_c (YBCO) or close to the irreversibility line (BSCCO) to avoid the influence of bulk pinning. Since we used polycrystalline samples of Hg-1212 and Hg-1223, it is more appropriate to compare with results from polycrystalline samples of other HTSC materials. For reasons described below, we have chosen a sample composed of fine, mostly monocrystalline $YBa_2Cu_3O_7$ particles produced by high-temperature pyrolysis of aerosols containing stoichiometric ratios of Y, Ba, and Cu cations in nitrate solutions. After synthesis, the randomly oriented YBCO particles were pressed at 6000 lb (27 000 N) into a cylinder with diameter of 4.8 mm and mass of 0.354 g. The sample was *not* sintered after pressing, in order to keep the intergrain connectivity poor. The magnetic onset T_c was 91 K and the average particle diameter, as revealed by scanning electron microscopy, was ~ 0.25 μm. Measurement of magnetization versus temperature in an applied field of 10 G showed that the field-cooled (FC) data were extremely similar to zero-field-cooled (ZFC) data.[24] In other words, the magnetization was highly reversible, suggesting that bulk-pinning effects are relatively weak. Given such a small grain size and high reversibility in low field, we expect the sample to have higher ratio of surface-pinning/bulk-pinning and hence[17] to show pronounced surface-pinning effects. Presented in Fig. 4 are magnetic hysteresis loops of the sample at $T=5$, 20, and 40 K. The shape of the loops is asymmetric with respect to the central line of $M=0$, which is infrequently seen in single crystals but often found in polycrystalline samples at higher temperatures. This indicates that the bulk pinning of these aerosol particles is very weak as expected. However, the loops lack a basic feature as compared with those in Fig. 1: the magnetization in the field-decreasing branch is not near zero, and it starts to increase at much larger fields. This indicates the surface pinning is too weak to resist flux lines escaping from the sample boundary; hence the magnetization lies near its equilibrium value $M_{eq}(H)$. In searching the literature we found that this feature is often seen for polycrystalline samples of YBCO and BSSCO measured at higher temperatures, e.g., $T > 30$ K, whereas at low temperatures, hysteresis loops are generally symmetric. From this point of view, the phenomena found in Hg-based superconductors are distinctive. It certainly demonstrates a much stronger surface barrier in Hg-based HTSC.

The answer to the first question, the tendency of Hg-based materials to have pronounced surface barriers, is not clear. Typically the surface barrier is considered a property of an individual sample, depending upon the method of sample preparation and the details of material processing. In our studies, samples made by different groups showed similar features. It may be due to some intrinsic properties associated with mercury, since the overall crystal structure and other elements in the Hg-based cupric oxides are similar to other HTSC; alternatively, it may arise from the low-temperature heat treatment in the solid-reaction method. This is a subject requiring further study.

Although the theory[9] of the surface barrier has been

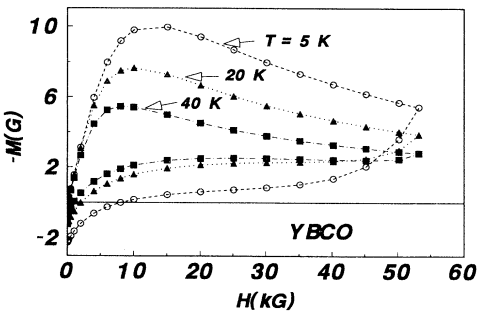

FIG. 4. M versus H for an assembly of small $Y_1Ba_2Cu_3O_7$ particles at $T=5$, 20, and 40 K.

developed since the early 1960's, few quantitative studies of the thickness of the vortex-free region and the density of the supercurrent flowing in this region, especially for HTSC's, are found in the literature. The Hg-based HTSC's provide a good chance for studying these questions. The following analysis of our experimental data locates the lower and upper boundaries of both quantities.

Considering a case where the bulk pinning is negligible and only the contribution from surface pinning is taken into account,[11,13] the algebraic value of the magnetization $M_{\rm in}$ (which is negative) in the field-increasing branch lies in the range of

$$M_{\rm en} \le M_{\rm in} \le M_{\rm eq} , \tag{2}$$

where $M_{\rm en}(H)$ is the entry magnetization at which the surface barrier is zero and $M_{\rm eq}(H)$ is the equilibrium magnetization. At a finite temperature, $M_{\rm in}$ relaxes from $M_{\rm en}$ toward $M_{\rm eq}$, causing the pinning energy to increase. If the surface barrier is weak, then $M_{\rm en}$ is close to $M_{\rm eq}$ and the relaxation is fast. Considering the field-decreasing branch with a strong surface barrier, flux lines are not free to exit until M_d (the magnetization in the field-decreasing branch) increases to zero. Hence M_d is within the range of

$$M_{\rm eq} \le M_d \le 0 . \tag{3}$$

The sum, $M_t(H)=M_{\rm in}(H)+M_d(H)$, equals to $M_{\rm en}$ for the limit of strong surface barrier and $2M_{\rm eq}$ for the weak limit. For a real system there are contributions from bulk pinning and background. The former has opposite signs but equal magnitudes for $M_{\rm in}$ and M_d. Hence the effects of bulk pinning in M_t just cancel. The magnetic background can be obtained by extrapolating the dependence of magnetization on temperature (Curie-Weiss law) measured above T_c. After subtracting the background magnetization, M_t involves contributions only from surface pinning. The magnetization due solely to the surface barriers *in the field-increasing branch,* labeled $M_{\rm ins}$ ($M_{\rm ds}$ in the field-decreasing branch), can be evaluated with M_t. For the strong limit of the surface barrier, one has $M_{\rm ds}=0$ so that M_t only involves $M_{\rm ins}$. For the weak limit, $M_{\rm ds}=M_{\rm eq}$ and $M_{\rm ins}=M_t-M_{\rm ds}\approx M_t-M_{\rm eq}$. Therefore we find

$$M_t(H)-M_{\rm eq}(H) \le M_{\rm ins}(H) \le M_t(H) . \tag{4}$$

As discussed in more detail in our earlier work[8] and references therein, the opposing forces on a vortex near the surface make this region energetically unfavorable. Consequently the near surface is vortex-free for a depth x_f. Having defined $M_{\rm ins}$ within these bounds, we are able to calculate x_f and J_s, the density of the persistent current flowing in the region. For a cylindrical sample with radius of R, we have

$$\begin{aligned} 4\pi M_{\rm ins} &= \frac{4\pi}{2V}\int_{R-x_f}^{R} r\times J dv = -\frac{1}{2Vc}\int_{R-x_f}^{R} r\frac{\partial h}{\partial r}dv = -H+B\left[1-\frac{x_f}{R}\right]^2 \\ &\quad + \frac{2\pi\lambda B[R\sinh(x_f/\lambda)+\lambda(1-H/B)]}{V} \\ &= (B-H)\left[1+2\left[\frac{\lambda}{R}\right]^2\right]+\cdots , \end{aligned} \tag{5}$$

where B is the vortex density at the boundary of the vortex-free region located at $r \ge R-x_f$, λ is the penetration depth (a-b plane), $h(r)=B\cosh[(x_f+r-R)/\lambda]$ and V is the volume per unit length of the cylindrical sample. The relations[11,13] $x_f=\lambda\cosh^{-1}(H/B)$ and $J_s=(4\pi/c)\nabla x h(r)$ have been used in the above calculations. In our case, $R\sim 5$ μm and $\lambda\approx 0.1$ μm, so we neglect the term $\sim(\lambda/R)^2$. Therefore we obtain

$$B(r=R-x_f)=H+4\pi M_{\rm ins} . \tag{6}$$

With values of B, calculations of x_f and J_s are straightforward.

To proceed, however, we need the equilibrium magnetization to evaluate the lower bound in Eq. (4). Hence, Fig. 5 shows the equilibrium magnetization of sample $O3$ measured in the reversible region, plotted versus $1-(T/T^*)^2$ with $T^*=127$ K. Over a wide range of temperature, the reversible magnetization depends linearly on $(T/T^*)^2$, similar to results for Hg-1212 reported by Huang *et al.*[25] Assuming the relation applies at lower temperatures, we obtain values of $M_{\rm eq}$ by extrapolation, which are used for calculating the lower boundary of $M_{\rm ins}$ via Eq. (4) (note that $M_{\rm eq}$ is small compared with M_t, so the results are relative insensitive to the details of the extrapolation). Results for the upper and lower boundaries of x_f/λ for sample $A3$ at $T=10$, 20, 30, and 40 K are plotted versus field in Fig. 6 and the inset, respective-

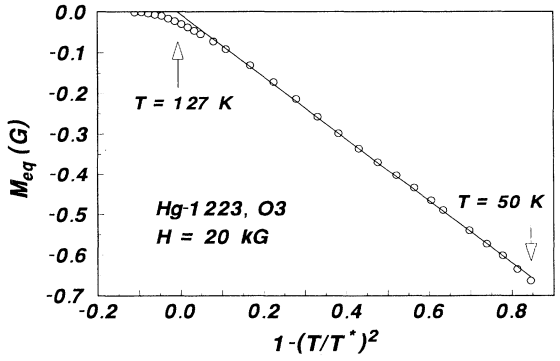

FIG. 5. Equilibrium magnetization $M_{\rm eq}$ versus $1-(T/T^*)^2$ at $H=20$ kG for sample $O3$.

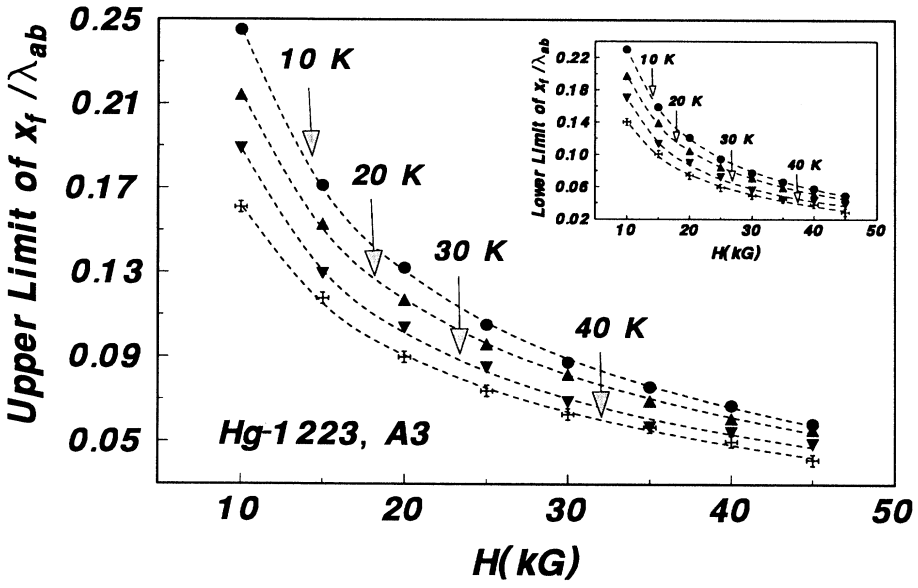

FIG. 6. The upper boundaries of x_f/λ_{ab} versus H at $T=10$, 20, 30, and 40 K for sample $A3$; inset: the corresponding values of the lower boundaries under the same conditions. Lines represent regression curves: $x_f/\lambda_{ab}=c_1/H+c_2+c_3H$ where c_1, c_2, and c_3 are fitting parameters.

ly; the dashed lines are smooth and empirical regression curves. In this temperature region, λ is almost a constant, so that x_f monotonically decreases with increasing field and temperature. For the field and temperature region shown, the range of x_f is $0.025\lambda_{ab} \leq x_f \leq 0.25\lambda_{ab}$. An earlier analysis[3] of dc magnetization of Hg-1201 yielded the value 0.12 μm for λ, the magnetic penetration depth corresponding to currents flow in the Cu-O plane. Subsequent ac response studies led the similar value for Hg-1223,[26] so we use value $\lambda=0.12$ μm for present calculations; this gives 3 nm $\leq x_f \leq$ 30 nm.

Since x_f is small, we can replaced the parabolic function of $h(x)$ in the vortex-free region with a linear function without losing much accuracy. Hence, $J_s=c(H-B)/4\pi x_f=cM_{\rm ins}/x_f$. By substituting the upper and lower boundaries with regression values of $M_{\rm ins}(H)$ and $x_f(H)$, we obtained the corresponding values of $J_s(H)$, which are plotted in Fig. 7 and the inset, respectively. The upper and lower limits give similar values for J_s and x_f mean they define these quantities rather well. The most impressive feature found in Fig. 7 is the high magnitude of J_s. At $T=40$ K, and $H=45$ kG, the lower boundary of J_s is about 4.5×10^7 A/cm^2. Furthermore, J_s is only weakly field dependent. Recalling that the supercurrent flows in a vortex-free region, we expect its reaction to the applied field to be similar to

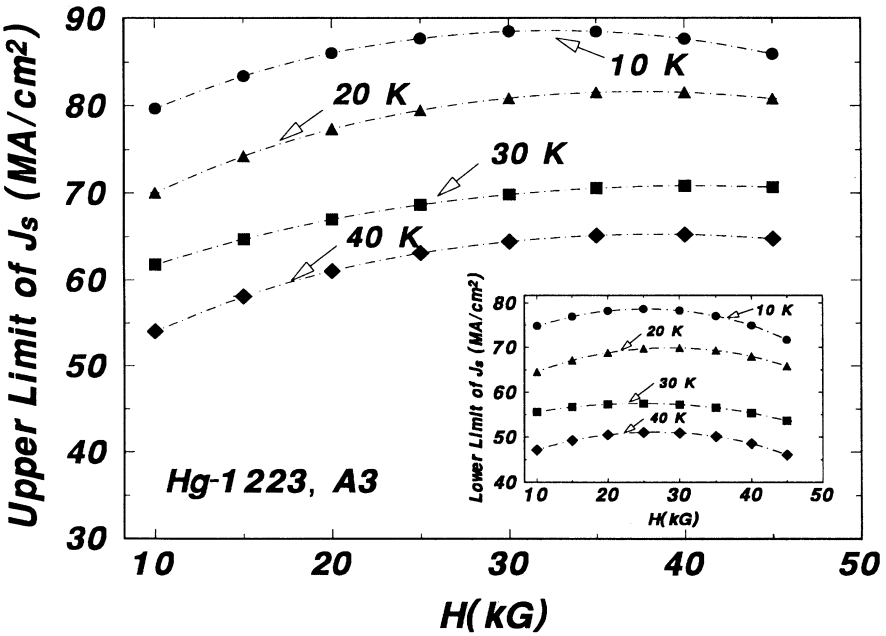

FIG. 7. The upper boundaries of the surface current density J_s versus H at $T=10$, 20, 30, and 40 K for Hg-1223 sample $A3$; inset: the corresponding values of the lower limit under the same conditions. J_s is calculated with regression values of x_f and $M_{\rm ins}$.

the screening current in the Meissner state rather than a Bean-like critical state; in the critical state, the critical current results from the balance between the Lorentz driving force and the pinning force on vortex bundles, while the former case has *no* vortices near the surface. Finally we note in Fig. 7 that the curves at different temperatures are separated approximately equally at the rate of ~ 1 MA/cm^2 K indicating a roughly linear dependence of J_s on temperature over the entire field range.

An interesting point was raised recently by Indenbom and co-workers[27] in interpreting the asymmetric magnetization curves in type-II superconductors, especially for thin films in a perpendicular magnetic field. They indicated that for a flat thin sample in a perpendicular field, the very large demagnetization factor means that the field at the sample edge becomes very large and decreases sharply near the sample surface.[27,28] This is rather similar to the exponential decay caused by a surface barrier. Comparing numerical studies with direct magneto-optical observations, they found that decreasing the applied field does not produce immediate decreasing of captured flux. In other words, the changing of the flux density inside the sample is delayed, which makes the magnetization in the return path close to zero. They call this a *barrierlike* effect, to distinguish it from the Bean-Livingston surface-barrier effect. However, in our case, the samples are polycrystalline with either a cylindrical shape ($O2$ and $O3$) or irregular shapes with nearly an equal size for length, width, and thickness ($A2$ and $A3$); this geometry is rather different from the situation in their studies. Furthermore, with a large applied field, the magnetization from intergrain currents is very small,[8] which makes the geometrical barrier effect negligible. Thus the observed magnetization originates primarily from intragrain current as analyzed in preceding paragraphs.

CONCLUSIONS

The Hg-based polycrystalline superconductors, in contrast to most other HTSC's to date, show striking effects of surface barriers over wide ranges of temperature and magnetic field. The influence of the surface barrier on flux pinning for grains is comparable to the effects of neutron-irradiation-generated vortex pinning. The surface current density J_s is weakly field dependent but declines linearly with the temperature. The high values of J_s in an ultrathin surface layer suggest the potential of applications for the materials in the future.

ACKNOWLEDGMENTS

We thank J. L. Wagner and D. G. Hinks at Argonne National Laboratory for providing samples and R. Holm, M. Kaczor, and G. W. Raban, Jr., at the University of Illinois at Urbana for assistance with performing the irradiation. We wish to express our appreciation to H. Hsu of Oak Ridge National Laboratory for supplying the fine, spray pyrolysis-produced $YBa_2Cu_3O_{7-\delta}$ powder. The work of Y.R.S. and J.S. was supported by U.S. National Science Foundation Contract No. DRM-91-200000 through the Science and Technology Center for Superconductivity and by the U.S. Department of Energy Basic Energy Sciences Material Sciences under Contract No. W-31-109-ENG-38 (D.G.H.). The Science Alliance at the University of Tennessee supported a portion of the work of J.R.T. For work performed at the Oak Ridge National Laboratory, the research was sponsored by the Division of Materials Sciences, U.S. Department of Energy and technology development was funded by the U.S. Department of Energy, Office of Advanced Utilities Concepts-Superconductivity Partnership Program, both under Contract No. DE-AC05-84OR21400 with Martin Marietta Energy Systems, Inc.

[1]S. N. Putilin, E. V. Antipov, O. Chmaisse, and M. Marezio, Nature (London) **362**, 226 (1993).

[2]J. L. Wagner, P. G. Radaelli, D. G. Hinks, J. D. Jorgensen, J. F. Mitchell, B. Dabrowski, G. S. Knapp, and M. A. Beno, Physica C **210**, 447 (1993); P. G. Radaelli, J. L. Wagner, M. A. Beno, G. S. Knapp, J. D. Jorgensen, J. F. Mitchell, and D. G. Hinks, *ibid.* **216**, 29 (1993).

[3]J. R. Thompson, J. G. Ossandon, D. K. Christen, B. C. Chakoumakos, Y. R. Sun, M. Paranthaman, and J. Brynestad, Phys. Rev. B **48**, 14 031 (1993).

[4]U. Welp, G. W. Crabtree, J. L. Wagner, D. G. Hinks, P. G. Radaelli, J. D. Jorgensen, J. F. Mitchell, and B. Dabrowski, Appl. Phys. Lett. B **63**, 693 (1993).

[5]Z. J. Huang, Y. Y. Xue, R. L. Meng, and C. W. Chu, Phys. Rev. B **49**, 4213 (1994).

[6]J. Schwartz, S. Nakamae, G. W. Raban, Jr., J. K. Heuer, S. Wu, J. L. Wagner, and D. G. Hinks, Phys. Rev. B **48**, 9932 (1993).

[7]L. Gao, Y. Y. Xue, F. Chen, Q. Xiong, R. L. Meng, D. Ramirex, C. W. Chu, J. H. Eggert, and H. K. Mao, Phys. Rev. Lett. **50**, 4260 (1994).

[8]Y. R. Sun, J. R. Thompson, H. R. Kerchner, D. K. Christen, M. Paranthaman, and J. Brynestad, Phys. Rev. B **50**, 3330 (1994).

[9]C. P. Bean and J. D. Livingston, Phys. Rev. Lett. **12**, 14 (1964).

[10]P. G. de Gennes, Solid State Commun. **3**, 127 (1965); also P. G. de Gennes, *Superconductivity of Metals and Alloys* (Benjamin, New York, 1966), p. 79.

[11]J. R. Clem, in *Proceedings of the 13th Conference on Low Temperature Physics (LT 13)*, edited by K. D. Timmerhaus, W. J. O'Sullivan, and E. F. Hammel (Plenum, New York, 1974), Vol. 3, p. 102.

[12]F. F. Ternovskii and L. N. Shekhata, Zh. Eksp. Teor. Fiz. **62**, 2297 (1972) [Sov. Phys. JETP. **35**, 1202 (1972)].

[13]L. Burlachkov, Phys. Rev. B **47**, 8056 (1993).

[14]J. Schwartz, J. Appl. Phys. **73**, 1343 (1993).

[15]M. Paranthaman, J. R. Thompson, Y. R. Sun, and J. Brynestad, Physica C **213**, 271 (1993).

[16]C. P. Bean, Phys. Rev. Lett. **8**, 250 (1962).

[17]M. R. Beasley, R. Labusch, and W. W. Webb, Phys. Rev.

181, 682 (1969).
[18]Y. Yeshurun and A. P. Malozemoff, Phys. Rev. Lett. **60**, 2202 (1987).
[19]D. R. Nelson, Phys. Rev. Lett. **60**, 1973 (1988).
[20]M. P. A. Fisher, Phys. Rev. Lett. **62**, 1415 (1989).
[21]L. Burlachkov, M. Konczykowski, Y. Yeshurun, and F. Holtzberg, J. Appl. Phys. **70**, 5759 (1991).
[22]S. T. Weir, W. J. Nellis, Y. Dalichaouch, B. W. Lee, M. B. Maple, J. Z. Liu, and R. N. Shelton, Phys. Rev. B **43**, 3034 (1991).
[23]N. Chikumoto, M. Konczykowski, N. Motohira, and A. P. Malozemoff, Phys. Rev. Lett. **69**, 1260 (1992).
[24]J. R. Thompson, D. K. Chirsten, H. R. Kerchner, L. A. Boatner, B. C. Sales, B. C. Chakoumakos, H. Hsu, J. Brynestad, D. M. Kroeger, J. W. Williams, Yang Ren Sun, Y. C. Kim, J. G. Ossandon, A. P. Malozemoff, L. Civale, A. D. Marwick, T. K. Worthington, L. Krusin-Elbaum, and F. Holtzberg, in *Magnetic Susceptibility of Superconductors and Other Spin Systems,* edited by R. A. Hein, T. Francavilla, and D. Liebenburg (Plenum, New York, 1992), p. 157.
[25]Z. J. Huang, Y. Y. Xue, R. L. Meng, and C. W. Chu, Phys. Rev. B **49**, 4218 (1994).
[26]M. Couach, A. F. Khoder, R. Caiemzuck, Ch. Marcenat, J. L. Tholence, J. J. Capponi, and M. F. Gorius, Phys. Lett. A (to be published).
[27]M. V. Indenbom, A. Forkl, and H. Kronmuller, Physica B **194-196**, 1927 (1994); also M. V. Indenbom and E. H. Brandt, Phys. Rev. Lett. **73**, 1731 (1994).
[28]E. Zeldov, J. R. Clem, M. McElfresh, and M. Darwin, Phys. Rev. B **49**, 9802 (1994).

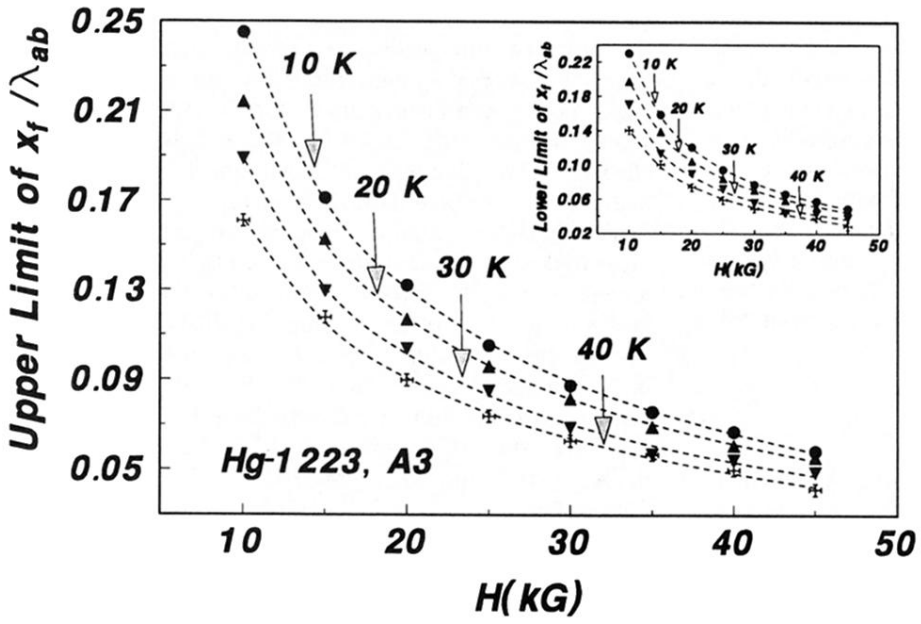

FIG. 6. The upper boundaries of x_f/λ_{ab} versus H at $T=10$, 20, 30, and 40 K for sample $A3$; inset: the corresponding values of the lower boundaries under the same conditions. Lines represent regression curves: $x_t/\lambda_{ab}=c_1/H+c_2+c_3H$ where c_1, c_2, and c_3 are fitting parameters.